Multistability and hysteresis phenomena in passively mode-locked fiber lasers

Andrey Komarov,* Hervé Leblond, and François Sanchez
Laboratoire POMA, UMR 6136, Université d'Angers, 2 Bd Lavoisier, 49000 Angers, France
(Received 4 February 2005; published 20 May 2005)

A passively mode-locked fiber laser is theoretically investigated. The mode locking is achieved using the nonlinear polarization technique. We consider the practical case of the ytterbium-doped fiber laser operating in the normal dispersion regime. The effect of the phase plates is explicitly taken into account. The resulting model reduces to one iterative equation for the optical Kerr nonlinearity, the phase plates and the polarizer, and one partial differential equation for the gain and the dispersion. Numerical simulations allow us to describe several features observed in passively mode-locked fiber lasers such as bistability between the mode lock and the continuous regime, multiple pulse behavior, hysteresis phenomena. The dynamics of the number of pulses as a function of the pumping power is also reported. Pump power hysteresis is demonstrated.

DOI: 10.1103/PhysRevA.71.053809 PACS number(s): 42.60.Fc, 42.65.Sf

I. Introduction

Self-started, passively mode-locked fiber lasers are very attractive from the dynamical point of view because they exhibit a large variety of behaviors. Indeed, in addition to the regular mode-locking regime which has been reported in different optical configurations, many regimes involving several pulses by cavity round trip have been observed or theoretically predicted. Experimental results were obtained with erbium-doped figure eight lasers [1–6]. Bunches of pulses were observed, pulses randomly spaced but well separated and also harmonic mode-locking, where the pulses are equally separated along the cavity. Other features such as *Q*-switch operation and bistability between the continuous and mode-lock regimes were also reported [4,5]. The evolution of the number of pulses as a function of the pump power was investigated in Ref. [5] where the authors showed that the pulses disappear one by one when the pump was decreased. Mode locking using the figure eight geometry has also been reported with praseodymium [7] and ytterbium [8] doped fibers. Bunches of pulses were also observed [7]. The possibility of exploiting the nonlinear polarization rotation to obtain passive mode locking was proposed by Mollenauer and a theoretical description was given in Ref. [9]. Experimental demonstration of mode locking through nonlinear polarization rotation was then demonstrated [10–12]. Here again, multiple pulsing was also observed although the basic principle of mode locking was different from the one of figure-8 lasers. In order to increase the energy per pulse the stretched-pulse configuration, which also allows reducing the pulse duration, was proposed [13]. This configuration leads to various dynamical behaviors such as bistability between the continuous (CW) and the mode-lock (ML) regime, harmonic mode locking, and multiple pulsing [13–16]. In particular, it was shown in Ref. [16] that a large bistability domain exists between the CW and the ML operating regimes. The evolution of the number of pulses versus the pumping power was deeply investigated and it was demonstrated that the pulses were created and annihilated one by one and also that a large hysteresis occurred when pump power was varied. Pulse splitting and multiple pulse operation have also been observed experimentally [17,18] and theoretically [19–21] in Ti-sapphire lasers. In the nonlinear polarization rotation based mode-locked lasers, additional behaviors such as bound states or pulse fragmentation can be observed by simply rotating one of the phase plates used in the polarization controller set [22–28]. Bound solitons have been also reported in figure-8 fiber lasers [29,30]. From the nonexhaustive review presented just above (complete reviews can be found in Refs. [31,32]), it appears that multiple pulsing, bistability between the CW and the ML regimes, *Q* switching, and locked pulses are common features in fiber lasers independently of the exact optical configuration. In addition, most of these operating regimes can be obtained by a simple rotation of a phase plate in the cavity.

From the theoretical point of view, first models were based on master equations which had the advantage to be simple but which did not allow us to take into account the essential role played by the phase plates [33–37]. The models consisted in writing a phenomenological scalar equation assuming that all effects per pass were small. They included the group-velocity dispersion (GVD), the optical Kerr nonlinearity, and a gain medium. The mode-locking properties of a fiber laser can be well described through this approach for positive and negative GVD. The effects of the phase plates cannot be described in this way. Other approaches based on two-coupled nonlinear equations have been also used [38,39]. More recently, a scalar model has been proposed for the mode-locking properties of the ytterbium-doped ring fiber laser passively mode locked through nonlinear polarization rotation [40] and it has been further extended to both negative GVD regime [41] and stretched-pulse regime [42]. This model includes the GVD, the birefringence, the optical Kerr nonlinearity, and linear gain (i.e., gain saturation effects were neglected). The master equation is of a complex cubic Ginzburg-Landau type and the coefficients explicitly take into account the orientation angles of the phase plates. The biggest advantage of this model is that it leads to analytical

*Permanent address: Institute of Automation and Electrometry, Russian Academy of Sciences, Acad. Koptyug Pr., 1, 630090, Novosibirsk, Russia.

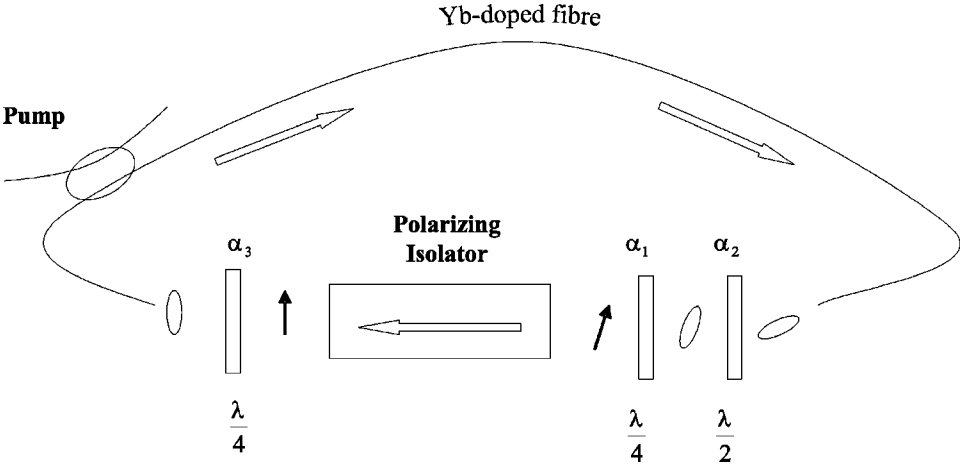

FIG. 1. Schematic representation of an ytterbium-doped fiber ring laser passively mode locked through nonlinear polarization rotation.

results for the mode-locking solutions and that the stability of the ML solutions can be studied as a function of the orientation of the phase plates. Its major drawback is that it is not possible to investigate the effect of the pumping power. Bound states were predicted from a complex Ginzbug-Landau equation [43,44]. More realistic models based on the experiment have been developed recently for the bound-state regimes [45]. In spite of the great amount of theoretical work, there is no model, to the best of our knowledge, related to the multiple pulse dynamics of a fiber laser.

The aim of this paper is to develop a simple theoretical model allowing us to describe the dynamics of multiple pulsing in a typical passively mode-locked fiber laser. The model is presented in Sec. II and considers the real case of an ytterbium-doped fiber ring laser passively mode locked through nonlinear polarization rotation and operating in the normal dispersion regime. It takes into account the optical Kerr nonlinearity, the GVD, the saturating gain, and the orientation of the phase plates. The final model consists in one algebraic equation accounting for the Kerr nonlinearity for the phase plates and for the polarizer, and a differential equation which includes the gain and the GVD. Numerical simulations are given in Sec. III. Bistability between the ML and the CW operating regimes is first demonstrated. We then demonstrate that in the ML regime, for a fixed position of the phase plates, new pulses can be generated one by one when the pump parameter is increased. Pump power hysteresis is shown in both normal and anomalous dispersion regimes. These results are in very good agreement with the corresponding experimental data of Ref. [16].

II. MODEL

A. Basic principles of the model

We consider an ytterbium-doped fiber ring laser operating in the normal dispersion regime and passively mode locked through nonlinear polarization rotation. The setup is shown in Fig. 1 [46]. For isotropic fibers this scheme involves all necessary elements for control of nonlinear losses. After the polarizing isolator the electric field has a linear polarization. Such a state of polarization does not experience polarization rotation in the fiber because the rotation angle is proportional to the area of the polarization ellipse. Consequently, it is necessary to place a quarter wave plate 3 (α_3 represents the orientation angle of one eigenaxis of the plate with respect to the laboratory frame). The rotation of the polarization ellipse resulting from the optical Kerr nonlinearity is proportional to the light intensity, the area of the polarization ellipse, and the fiber length [47]. At the output of the fiber, the direction of the elliptical polarization of the central part of the pulse can be rotated towards the passing axis of the polarizer by the half wave plate 2 (the orientation angle is α_2). Then this elliptical polarization can be transformed into a linear one by the quarter wave plate 1 (the orientation angle is α_1). In this situation the losses for the central part of the pulse are minimum while the wings undergo strong losses. In the following, we model the setup of Fig. 1 as follows. The fiber is assumed to have GVD, optical Kerr nonlinearity, and saturable gain. Linear birefringence is not taken into account in our model since it is not required for mode locking or for multiple pulsing. In a first step we solve the equations for a field propagating in a Kerr medium and take into account the three phase plates and the polarizer. After that, we write a scalar equation of a wave propagating in a saturable amplifying medium with GVD. The resulting model assumes a localized effect for the nonlinear loss due to the Kerr nonlinearity and the phase plates and distributed gain and GVD.

B. Nonlinear polarization rotation and the phase plates

Let us consider a wave packet propagating along the z axis in a fiber exhibiting Kerr nonlinearity and without linear birefringence. For large peak powers, the nonlinear effects are large enough, so that the effect of the amplification and the frequency gain filtering together with the GVD on one round trip can be neglected in a first approximation. They will be taken into account in a second step, as perturbations which have an essential effect on a large number of round trips. With this assumption, the propagation equations for the electric field components in the laboratory frame are the same as for a plane wave, i.e., Refs. [40,47]:

$$\frac{\partial u}{\partial z} = i\gamma(|u|^2 u + A|v|^2 u + Bv^2 u^*),$$

$$\frac{\partial \nu}{\partial z} = i\gamma(|\nu|^2\nu + A|u|^2\nu + Bu^2\nu^*), \tag{1}$$

where $\gamma\,(\mathrm{W}^{-1}\,\mathrm{m}^{-1})$ is the nonlinear coefficient related to the nonlinear index coefficient n_2, and $A=2/3$ and $B=1/3$ for silicate fibers [47].

System (1) admits two conserved quantities:

$$I = |u(z)|^2 + |\nu(z)|^2 = |u(0)|^2 + |\nu(0)|^2, \tag{2}$$

$$J = \mathrm{Im}[u(z)\nu^*(z)] = \mathrm{Im}[u(0)\nu^*(0)]. \tag{3}$$

Relation (2) stands for the conservation of the energy I along the fiber while relation (3) shows the conservation of the area J of the polarization ellipse during the propagation along the fiber. Relation (3) is valid under the assumption that $A+B=1$, which is satisfied in silicate fibers.

With the help of conservation relations (2) and (3), the solutions of Eq. (1) can be straightforwardly calculated, as

$$\begin{pmatrix} u(z) \\ \nu(z) \end{pmatrix} = e^{i\gamma Iz}\begin{pmatrix} \cos\Omega z & \sin\Omega z \\ -\sin\Omega z & \cos\Omega z \end{pmatrix}\begin{pmatrix} u(0) \\ \nu(0) \end{pmatrix} = W\begin{pmatrix} u(0) \\ \nu(0) \end{pmatrix}, \tag{4}$$

where $\Omega=2\gamma BJ$ is a constant. Relation (4) shows that the polarization ellipse is rotated with a constant velocity Ω without any change of its shape during the propagation along the fiber. Ω is proportional to the ellipse area J, which depends on both the polarization state and the light intensity. For example, $\Omega=0$ for a linear incident polarization, in which case the fiber does not lead to nonlinear losses.

The phase plates are treated with the help of the Jones matrix formalism. In the framework of their eigenaxis, the Jones matrices of a half wave and a quarter wave plates are, respectively,

$$W_{\lambda/2} = \begin{pmatrix} -i & 0 \\ 0 & i \end{pmatrix}, \quad W_{\lambda/4} = \frac{1}{\sqrt{2}}\begin{pmatrix} 1-i & 0 \\ 0 & 1+i \end{pmatrix}. \tag{5}$$

Let M_k the Jones matrix of the phase plate number k ($k=1,2,3$) in the laboratory frame,

$$M_k = R(\alpha_k)W_kR(-\alpha_k), \tag{6}$$

where

$$R(\alpha) = \begin{pmatrix} \cos\alpha & -\sin\alpha \\ \sin\alpha & \cos\alpha \end{pmatrix} \tag{7}$$

is the rotation matrix of angle α and W_k stands for $W_{\lambda/2}$ or $W_{\lambda/4}$ depending on the phase plate under consideration.

Without loss of generality, the passing axis of the polarizer is assumed to be parallel to the x axis. Its Jones matrix is

$$M_P = \begin{pmatrix} \beta & 0 \\ 0 & 0 \end{pmatrix}, \tag{8}$$

where β is the transmission coefficient of the polarizer.

Just after the polarizer the electric field is polarized along the x axis and can be written

$$\begin{pmatrix} f_n(t) \\ 0 \end{pmatrix}.$$

The amplitude of the electric field at the $(n+1)$th round trip, f_{n+1}, can then be easily calculated as a function of its amplitude at the nth round trip through the relation

$$\begin{pmatrix} f_{n+1}(t) \\ 0 \end{pmatrix} = M_PM_1M_2WM_3\begin{pmatrix} f_n(t) \\ 0 \end{pmatrix}. \tag{9}$$

For a fiber of length L, we obtain $\Omega=\gamma B|f_n|^2\sin 2\alpha_3$ and

$$f_{n+1}(t) = -\beta e^{i\gamma|f_n|^2L}[\cos(\Omega L+\alpha)\cos(\alpha_1-\alpha_3) + i\sin(\Omega L+\alpha)\sin(\alpha_1+\alpha_3)]f_n(t), \tag{10}$$

where $\alpha=2\alpha_2-\alpha_1-\alpha_3$.

Relation (10) stands for the fast saturable absorption resulting from the combination of the nonlinear polarization rotation and the polarizer. In other words, Eq. (10) can be viewed as a nonlinear loss term.

C. Positive feedback and wave plate orientation

For the discussion it is convenient to use

$$I_{n+1} = \beta^2[\cos^2(pI_n+\alpha)\cos^2(\alpha_1-\alpha_3) + \sin^2(pI_n+\alpha)\sin^2(\alpha_1+\alpha_3)]I_n, \tag{11}$$

which is deduced from relation (10), setting $I_n=\gamma L|f_n|^2$ and $p=B\sin 2\alpha_3$. The nonlinear losses are due to the terms involving $(pI_n+\alpha)$. This dependency vanishes if $\cos^2(\alpha_1-\alpha_3)=\sin^2(\alpha_1+\alpha_3)$, that is, if $\cos 2\alpha_1\cos 2\alpha_3=0$. This condition is fulfilled if $\alpha_1=\pm\pi/4$ or $\alpha_3=\pm\pi/4$. On the other hand, the maximum transmission coefficient is obtained when

$$\cos^2(pI_n+\alpha)\cos^2(\alpha_1-\alpha_3) + \sin^2(pI_n+\alpha)\sin^2(\alpha_1+\alpha_3) = 1. \tag{12}$$

If $\cos^2(pI_n+\alpha)\neq 0$ and $\sin^2(pI_n+\alpha)\neq 0$, the maximum of the transmission is realized when both $\cos^2(\alpha_1-\alpha_3)$ and $\sin^2(\alpha_1+\alpha_3)$ reach their maximum value equal to 1. Unfortunately, in this case the nonlinear dependence on the intensity is absent. Thus, for the more contrast dependence of the transmission versus the intensity, it is necessary that either $\cos^2(\alpha_1-\alpha_3)$ or $\sin^2(\alpha_1+\alpha_3)$ is equal to zero. These conditions are fulfilled in the following cases:

$$f_{n+1}(t) = -\beta e^{i\gamma|f_n|^2L}\cos(p\gamma L|f_n|^2+\alpha)\cos(\alpha_1-\alpha_3)f_n(t), \quad \alpha_1+\alpha_3 = 0, \pm\pi, \tag{13}$$

$$f_{n+1}(t) = -i\beta e^{i\gamma|f_n|^2L}\sin(p\gamma L|f_n|^2+\alpha)\sin(\alpha_1+\alpha_3)f_n(t), \quad \alpha_1-\alpha_3 = \pm\pi/2. \tag{14}$$

Let us consider, for example, the case $\alpha_1+\alpha_3=0$, and assume that p is positive, i.e., $0<\alpha_3<\pi/2$ or $-\pi<\alpha_3<-\pi/2$. In the ranges $-\pi/2<pI_n+\alpha<0$ and $\pi/2<pI_n+\alpha<\pi$, the nonlinear transmission works as a positive feedback: the greater intensity produces the lower losses. On the other hand, in the ranges $0<pI_n+\alpha<\pi/2$ and $-\pi<pI_n+\alpha<-\pi/2$, the nonlinear transmission acts as a negative feed-

back, i.e., the highest intensity creates the highest losses. The results are inverted if $p<0$. Of course, the mode locking requires a positive feedback. The positive feedback is controlled by changing either $\alpha_2=\alpha/2$ or α_3, which modifies p.

D. Dispersion and gain

The nonlinear losses are taken into account with relation (10), while the effect of dispersion, gain, and spectral gain filtering has be neglected. It can be treated as a perturbation on a single round trip, the effect of which on a large number of round trips can be written as a differential equation for the amplitude f of the electric field immediately after the polarizer [40]. This equation is formally the same as the propagation equation of the electric-field amplitude in a dispersive fiber with saturable gain and no Kerr nonlinearity. In the frame moving at the group velocity, the latter is [47]

$$\frac{\partial f}{\partial z}=\left(\rho-i\frac{\beta_2}{2}\right)\frac{\partial^2 f}{\partial t^2}+gf, \tag{15}$$

where β_2 ($\mathrm{ps^2\,m^{-1}}$) is the second-order GVD. The saturated gain g ($\mathrm{m^{-1}}$) has the expression

$$g=\frac{g_0}{1+\dfrac{1}{P_{sat}T_a}\displaystyle\int|f|^2dt}, \tag{16}$$

in which $T_a=L/c$ (s) is the photon round trip time, g_0 ($\mathrm{m^{-1}}$) is the unsaturated gain, and P_{sat} (W) is the saturating power. $P_{\mathrm{sat}}=(h\nu\pi r^2)/(\sigma T_1)$, where $h\nu$ (J) is the photon energy, σ ($\mathrm{m^2}$) is the stimulated emission cross section, T_1 (s) is the lifetime of the upper level of the lasing transition, and r (m) is the radius of the fiber core. The spectral filtering is $\rho=g/\omega_g^2+\rho_c$, where ω_g ($\mathrm{s^{-1}}$) is the spectral gain bandwidth. Here, in addition to the spectral gain filtering g/ω_g^2, we introduce phenomenologically the term ρ_c, which describes the frequency dispersion for the transmission due to both additional spectrally selective elements for control of a radiation spectrum or uncontrolled spectrally selective losses related with intracavity elements. This additional term is needed to obtain multiple pulsing regimes.

E. Normalization and numerical procedure

We introduce dimensionless variables related to the physical quantities through

$$\mathcal{E}=\frac{f}{\sqrt{I_r}},\quad \zeta=\frac{z}{L},\quad \tau=\frac{t}{\delta t}, \tag{17}$$

where $I_r=1/\gamma L$ and $\delta t=\sqrt{|\beta_2|L/2}$. Using the dimensionless variables, Eq. (10) becomes

$$\mathcal{E}_{n+1}(\tau)=-\beta e^{iI_n}[\cos(pI_n+\alpha)\cos(\alpha_1-\alpha_3)+i\sin(pI_n+\alpha)\sin(\alpha_1+\alpha_3)]\mathcal{E}_n(\tau), \tag{18}$$

where $I_n=|\mathcal{E}_n|^2$ and $p=B\sin 2\alpha_3$, as above. Equation (15) takes the form

$$\frac{\partial\mathcal{E}}{\partial\zeta}=(D_r+iD_i)\frac{\partial^2\mathcal{E}}{\partial\tau^2}+\frac{a}{1+b\displaystyle\int Id\tau}\mathcal{E}, \tag{19}$$

where $D_i=-\mathrm{sgn}(\beta_2)$ (in the normal dispersion regime $D_i=-1$, and in the anomalous dispersion regime $D_i=+1$), $D_r=2\rho/|\beta_2|$, $b=I_r\delta t/(P_{sat}T_a)$, and $a=g_0L$ is the pumping parameter.

The exponential factor in Eq. (18) is related to a nonlinear phase shift. The other factor describes the nonlinear transmission of the system involving the fiber, the phase plates, and the polarizing isolator. We remove this nonlinear phase shift from Eq. (18) and introduce it in the propagation equation in a gain and dispersive medium using the transform

$$E=\mathcal{E}e^{i\int^{\zeta}Id\zeta'}. \tag{20}$$

Relation (19) becomes

$$\frac{\partial E}{\partial\zeta}=(D_r+iD_i)\frac{\partial^2 E}{\partial\tau^2}+(G+i|E|^2)E, \tag{21}$$

where we have set for shortening $G=a/(1+b\int Id\tau)$. Then $D_r=GD_r^0+d_r$, with $D_r^0=2/(|\beta_2|L\omega_g^2)$ and $d_r=2\rho_c/|\beta_2|$. Equation (21) includes the nonlinear phase shift. Making the approximation $\int_{\zeta_n}^{\zeta_{n+1}}Id\zeta'\approx I_n(\zeta_{n+1}-\zeta_n)=I_n$, which is consistent with the previous ones, relation (18) is transformed into

$$E_{n+1}(\tau)=-\beta[\cos(pI_n+\alpha)\cos(\alpha_1-\alpha_3)+i\sin(pI_n+\alpha)\sin(\alpha_1+\alpha_3)]E_n(\tau). \tag{22}$$

The numerical procedure starts from the evaluation of the electric field after passing through the Kerr medium, the phase plates and the polarizer, using Eq. (22). The resulting electric field is then used as the input field to solve Eq. (21) over a distance L, using a standard split-step Fourier algorithm. The computed output field is used as the new input for Eq. (22). This iterative procedure is repeated until a steady state is achieved.

III. NUMERICAL SIMULATIONS

For the numerical simulations we consider the case of an ytterbium-doped fiber laser operating in the normal dispersion regime. The values of the different parameters are $\gamma=3\times10^{-3}\ \mathrm{W^{-1}\,m^{-1}}$ [47], $L=9$ m, $c=3\times10^8\ \mathrm{ms^{-1}}$, $\beta_2=0.026\ \mathrm{ps^2\,m^{-1}}$ [46], $\omega_g=10^{13}\ \mathrm{s^{-1}}$ [46], $r=5\times10^{-6}$ m, $\sigma=2.5\times10^{-24}\ \mathrm{m^2}$, $T_1=8\times10^{-4}$ s, and $\beta=0.95$.

A. Effect of the nonlinear feedback

It has been shown in Sec. II C that mode locking requires a positive nonlinear feedback: the greater intensity produces the lower losses. From Eq. (11) we obtain the nonlinear transmission coefficient $\eta=I_{n+1}/I_n$, as

$$\eta=\beta^2[\cos^2(\alpha_1-\alpha_3)-\cos 2\alpha_1\cos 2\alpha_3\sin^2\times(pI_n+2\alpha_2-\alpha_1-\alpha_3)]. \tag{23}$$

Recall that $p=B\sin 2\alpha_3$. A variation of intensity $\delta I=I-I_0$

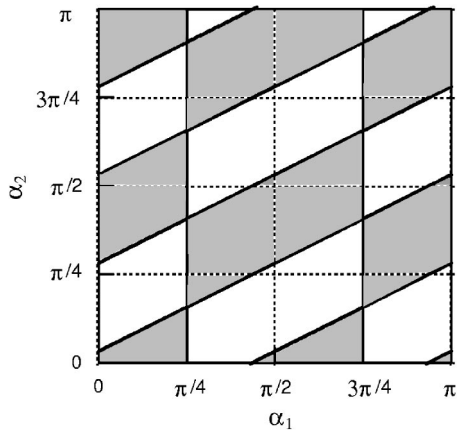

FIG. 2. Regions of positive (grey) and negative (white) nonlinear feedback as a function of orientation angles α_1 and α_2. The parameters used are $\alpha_3=0.2$ and $I_0=0$.

produces a variation of the transmission $\delta\eta=\eta'\delta I$ with

$$\eta' = \frac{1}{2}B\beta^2 \sin 4\alpha_3 \cos 2\alpha_1 \sin 2(pI_0 + 2\alpha_2 - \alpha_1 - \alpha_3). \tag{24}$$

The nonlinear transmission η' depends on the orientation angles α_1, α_2, α_3, and on the intensity I_0. For $\eta'<0$ the negative feedback is realized, the passive mode locking is not possible, and continuous operation occurs. The condition $\eta'>0$ is necessary for passive mode locking (but it is not sufficient). The zone map for positive and negative values of η' is presented in Fig. 2.

The boundaries of the zone are straight lines $\alpha_1=\pi/4+k\pi/2$ and $\alpha_2=\alpha_1/2+k\pi/4+\alpha_3/2-pI_0/2$, where k is an integer. For large intensities, the boundaries are considerably shifted, thus the condition for realization of passive mode locking is different for small and large intensities. A direct consequence is the existence of bistability between the continuous operation and the mode-locked regime. The nonlinear refractive index produces a frequency chirp proportional to the peak intensity of the pulse, and its spectrum is broadened. As a result, the efficiency of the amplification in the active medium decreases because of the finite spectral gain bandwidth. Thus there occurs the mechanism of negative feedback: the greater intensity produces the less amplification. For passive mode locking the net feedback must be positive. As a consequence, the sizes of the regions where mode locking occurs are smaller than the grey regions in Fig. 2.

The competition between the positive transmission feedback and the negative phase modulation feedback produces an additional mechanism of bistability between mode locking and CW operation, multiple pulse operation, and hysteresis phenomena.

For efficient operation, mode locking also requires a contrasted feedback. We consider the case corresponding to relation (13) with $\alpha_1+\alpha_3=0$, $\alpha_3=-\alpha_1=0.2$. The remaining phase plate allows us to control the value of α, which is taken equal to -0.7. These values completely fix the optical

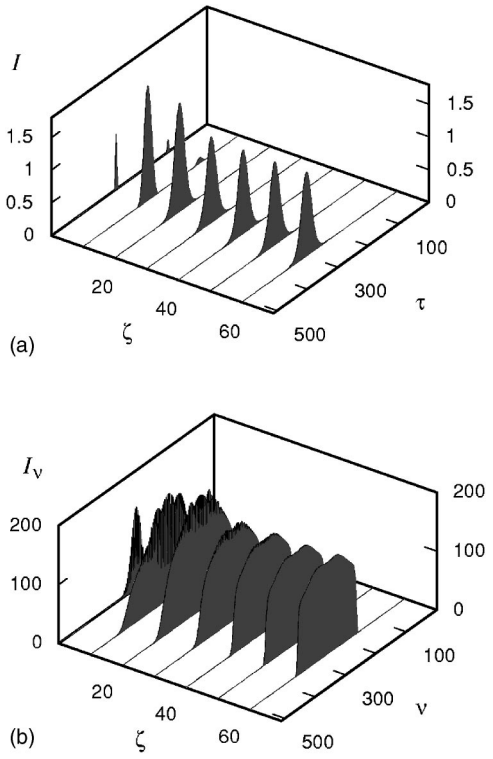

FIG. 3. Transient evolution of the field in the fiber laser. (a) Time distribution of the intensity I versus the round-trip number ζ, (b) spectral distribution of the field. The parameters used are $a=0.6$, $\alpha_3=-\alpha_1=0.2$, $\alpha=-0.7$, and $d_r=0$.

cavity and, in particular, the laser threshold that is $a_{th}=0.4$. Figure 3 shows the transient evolution of an initial pulse in the fiber laser [Fig. 3(a)] together with the evolution of the corresponding optical spectrum [Fig. 3(b)]. The pump parameter is $a=0.6$ and the spectrally selective losses are $d_r=0$. In this figure, ζ represents the number of round trips of the pulse in the cavity. The pulse duration is $T=12.9$ ps while the pulsewidth–spectral bandwidth product is 2.5. The peak power reaches $P_0=48$ W, and the pulse energy in the resonator is $E=0.6$ nJ. The optimization of the pulse duration is obtained with $d_r\neq 0$. The wings of the pulse have considerable detuning from the center frequency of the gain. The additional spectrally selective element suppresses detuning spectral components, cuts off the wings, and shortens the pulse. With this term, we obtain pulses as short as 1 ps.

When the pump parameter is increased, the peak intensity of the pulse increases and reaches the critical value such that $p|E|^2+\alpha=0$ for which the positive nonlinear feedback becomes negative. As a consequence, the increase of the peak intensity versus a is stopped and the pulse begins to lengthen. This behavior is presented in Fig. 4.

B. Bistability between the mode-locked and the continuous regimes

We consider here the possibility to obtain bistability between the passive mode locking and the continuous operation. The results of the numerical simulations are given in Fig. 5. The same parameters are used for both cases except-

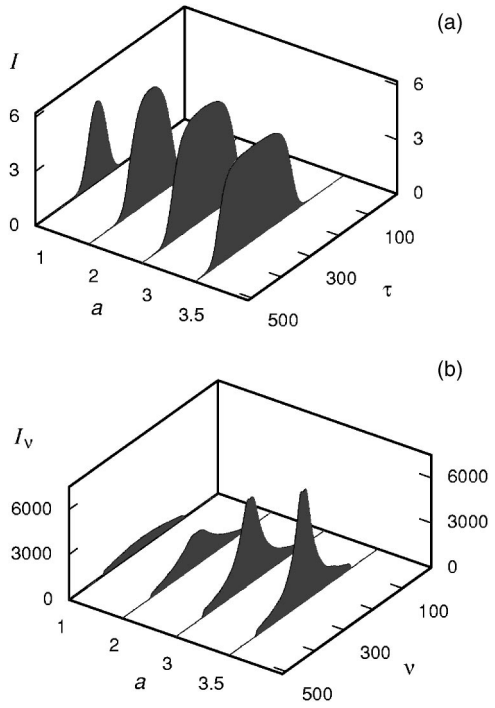

FIG. 4. Spatial (a) and spectral (b) distributions of the electric field for steady-state operation as a function of the pumping parameter a. The parameters used are the same as in Fig. 2.

ing the initial data. When using parameters for small peak intensity the nonlinear loss works as the negative feedback, all pulses decrease, and the continuous operation is established after transient evolution [Fig. 5(b)]. With powerful initial conditions the positive feedback is achieved and mode locking with single pulse occurs [Fig. 5(a)]. These results are in good agreement with experimental results observed in passively mode-locked fiber lasers [4,5,13,16].

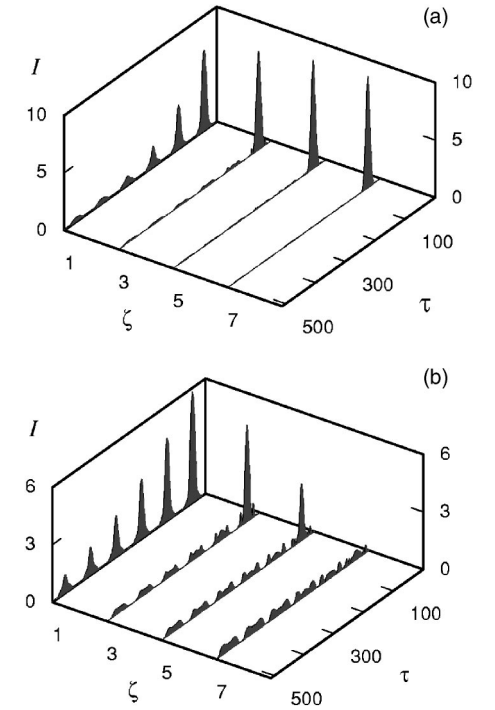

FIG. 5. Bistable operation: (a) passive mode locking vs (b) continuous operation. The parameters used are $a=2$, $\alpha=1.3$, $\alpha_1=0$, $\alpha_3=0.2$, and $d_r=0.2$.

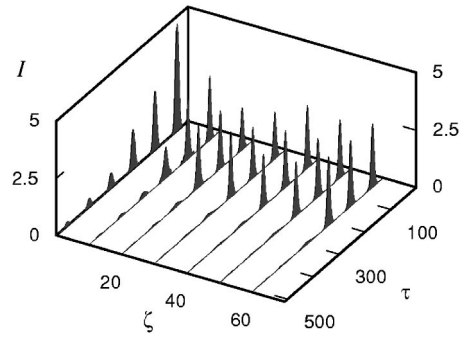

FIG. 6. Multiple pulse operation. The parameters used are $a=1.2$, $d_r=0.2$. The other parameters are the same as in Fig. 3.

C. Multistability and hysteresis phenomena in the multiple pulses regime

The sensitivity to the initial conditions suggests the existence of several attractors for a given set of parameters. In this section we are interested in multiple pulse operation of the laser and in the dynamics versus the pumping parameter. In the framework of our model, multiple pulsing requires additional spectrally selective losses, i.e., $d_r \neq 0$. Figure 6 shows an example of multiple pulses consisting in a bunch of three pulses. The pumping parameter is $a=1.2$. At this stage, it is interesting to investigate the evolution of the operating regime when the pumping parameter is varied. It is convenient to represent the results in a diagram which gives the number of pulses N for increasing and decreasing values of the pumping parameter. Results of the simulations are given in Fig. 7 in the normal dispersion regime. The pump parameter at lasing threshold is $a_{\text{th}}=0.68$. Several interesting features can be seen in this diagram. For increasing pumping, the laser is first continuous and then directly falls in a multiple pulsing regime ($N=3$) for a pump parameter $a_{\text{ML}}=2.1$. If the pump parameter is further increased, the number of pulses increases. The dynamics is different if now the pump is decreased. Indeed, the number of pulses disappears one by

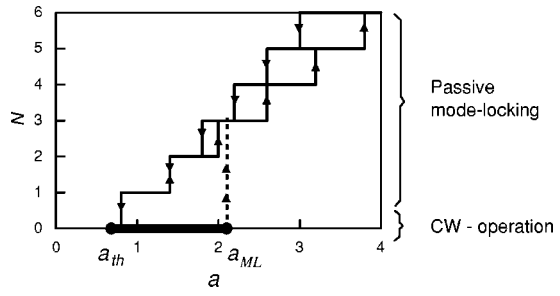

FIG. 7. Hysteresis dependence of the lasing regime and of the number N of pulses in steady-state operation on pumping a in the normal dispersion regime ($D_i=-1$). The parameters used are $\alpha=0.2$, $\alpha_1=-1.9$, $\alpha_3=0.2$, and $d_r=0.2$.

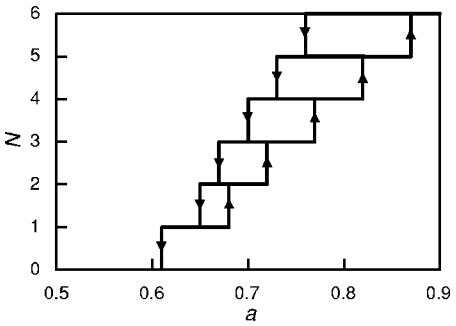

FIG. 8. Hysteresis dependence of the lasing regime and of the number of pulses in steady-state operation on pumping a in the anomalous dispersion regime ($D_i=+0.5$). The parameters used are $\alpha=0.3$, $\alpha_1=-1.9$, $\alpha_3=0.2$, and $d_r=0.2$.

one for particular values of a. This occurs until the laser becomes continuous again, for a value of the pump parameter close to its threshold value a_{th}. Moreover, when the laser is in the N-pulse mode-locked regime, the value of the pump parameter for which one additional pulse appears by increasing a is different from those obtained when a is decreased. Hence the formation and annihilation of each pulse show pump power hysteresis. The more pulses exist in the cavity, the bigger the hysteresis. Similar results are obtained in the anomalous dispersion regime as shown in Fig. 8.

In the case of the bistability between passive mode-locking and CW operation which is presented in Fig. 7, the nonlinear loss works as the positive feedback for both small and large intensities. Therefore the positive feedback increases with increasing intensity. However, with regard to the negative phase-modulation feedback, the net feedback is negative for small intensities and positive for large ones. As a result, at small intensity level, all ultrashort pulses in the cavity are suppressed and the CW operation is realized. On the contrary, at high intensity level, the net positive feedback selects the most powerful pulse and passive mode locking is established. An analogous bistability due to the change of the sign for the feedback with increasing intensity because of parasitic frequency-dependent loss was thoroughly studied in Ref. [48].

D. A qualitative explanation of multistability and hysteresis

At sufficiently high intensity level the nonlinear transmission η acts as the negative feedback: the greater intensity produces the less transmission. The transient evolution and steady-state operation are determined by a competition of pulses with different peak intensities. At the final stage of the transient process these pulses have equilibrium frequency chirp and duration, which are determined by the nonlinear-dispersion parameters of the laser and by the peak intensity of the pulses.

The difference $\Lambda=\lambda-G$ between the gain coefficient or growth rate λ for such equilibrium pulses and the linear gain G has the qualitative evolution shown in Fig. 9. This dependence corresponds to the dependence of the feedback on peak intensity of pulses: for small intensities the net feedback is negative, for greater intensity it is positive, and for

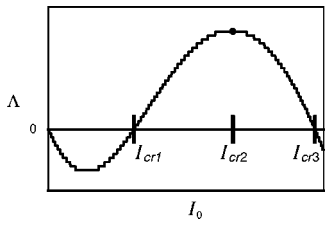

FIG. 9. Dependence of the amplification coefficient Λ due to nonlinear-dispersion laser parameters for pulses with equilibrium duration and frequency chirp on their peak intensity I_0 under competition pulses during the transient evolution.

higher intensity it is again negative. The dependence shown in Fig. 9 gives an insight into the properties of steady-state operation presented in Fig. 7 [20]. For self-starting of passive mode locking the peak intensity I_0 of one pulse must be greater than I_{cr1}. In the opposite case the pulses with small amplitudes will grow up from spontaneous emission, the laser cavity is filled by radiation and CW operation is established.

In the case of passive mode-locking operation with increasing pump power, the number of pulses in the steady-state operation will be increased. More precisely, for peak intensities $I_{\text{cr3}}>I_0>I_{\text{cr2}}$, the pulse with the greatest intensity is less amplified than the less powerful one; thus the amplitudes of these pulses are equalized as it is shown in Fig. 3. Furthermore, with increasing pump power the common peak intensity of the steady-state pulses increase. When it becomes greater than I_{cr3}, then Λ becomes negative, which means that the pulses are less amplified than the CW background. Therefore a new pulse arises from the background instability. As this takes place, the peak intensities of the steady-state pulses become less than I_{cr3} because of energy balance. With further increasing pump power the peak intensities of these pulses increase and reach again the level I_{cr3}, and then next pulse arises in generation, and so on. This process explains the lower stepwise curve in Fig. 7.

In the case of multiple pulse operation with decreasing pump power the peak intensities of all pulses are the same and decrease. As long as their peak intensities are greater than I_{cr2}, the number of these pulses does not change. This process is described by horizontal lines in Fig. 7. When the peak intensities of pulses reach the value I_{cr2} then, because of perturbations, the peak intensity of one of them becomes less than I_{cr2} and enters the domain of net positive feedback: the pulse with the lowest intensity undergoes less amplification, and therefore this pulse is suppressed. Then the peak intensities of the remaining pulses become greater than I_{cr2} because of energy balance. With further decreasing pump power the peak intensities of these pulses decrease and reach again the level I_{cr2} and then successive pulse is suppressed, and so on. This process explains the upper stepwise curve in Fig. 7.

Multiple pulse operation, multistability, and hysteresis were previously described and investigated in Kerr-lens mode-locked Ti:sapphire lasers [17–21]. Our theoretical results are in very good agreement with experimental data obtained in passively mode-locked fiber lasers [2–5,10,11,16].

IV. CONCLUSIONS

In this paper we have developed a theoretical model to describe several behaviors which are usually observed in passively mode-locked fiber lasers. The model is based on a fiber exhibiting optical Kerr nonlinearity, group velocity dispersion, and saturable gain. The cavity includes three phase plates and a polarizer in order to mode lock the laser through the nonlinear polarization rotation technique. The final form of the model consists in an iterative equation taking into account the Kerr nonlinearity, the phase plates, and the polarizer, and a partial differential equation related to the gain and the GVD. We have also included additional frequency selective losses which are necessary to model multiple pulsing regimes and hysteresis phenomena. Gain saturation as well as orientation of the phase plates is explicitly included. The model is simple and is not computer time consuming. The role of the nonlinear losses in the mode-locking properties has been established. Positive nonlinear feedback is required to obtain passive mode locking. We have then demonstrated that bistability occurs between the passive mode-locking regime and the continuous regime. Multiple pulse operation has been pointed out. The evolution of the number of pulses as a function of the pumping parameter has been carefully investigated. In particular, we have shown that the pulses appear one by one when the pump is increased and that large pump power hysteresis exists. These different behaviors have been explained as a consequence of the competition between the positive nonlinear feedback and the negative phase modulation effect.

Although our results are in good agreement with experimental data reported in the literature, it remains additional work to describe the main behaviors experimentally observed in passively mode-locked fiber lasers. *Q* switching and other hysteresis phenomena are yet to be theoretically investigated. These problems are actually under study.

[1] A. G. Bulushev, E. M. Dianov, and O. G. Okhotnikov, Opt. Lett. **16**, 88 (1991).
[2] D. J. Richardson, R. I. Laming, D. N. Payne, M. W. Phillips, and V. J. Matsas, Electron. Lett. **27**, 730 (1991).
[3] D. J. Richardson, R. I. Laming, D. N. Payne, V. J. Matsas, and M. W. Phillips, Electron. Lett. **27**, 1451 (1991).
[4] M. Nakazawa, E. Yoshida, and Y. Kimura, Appl. Phys. Lett. **59**, 2073 (1991).
[5] A. B. Grudinin, D. J. Richardson, and D. N. Payne, Electron. Lett. **28**, 67 (1992).
[6] M. J. Guy, D. U. Noske, and J. R. Taylor, Opt. Lett. **18**, 1447 (1993).
[7] M. J. Guy, D. U. Noske, A. Boskovic, and J. R. Taylor, Opt. Lett. **19**, 828 (1994).
[8] A. V. Avdokhin, S. V. Popov, and J. R. Taylor, Opt. Express **11**, 265 (2003).
[9] C.-J. Chen, P. K. A. Wai, and C. Menyuk, Opt. Lett. **17**, 417 (1992).
[10] V. J. Matsas, T. P. Newson, D. J. Richardson, and D. N. Payne, Electron. Lett. **28**, 1391 (1992).
[11] D. U. Noske, N. Pandit, and J. R. Taylor, Electron. Lett. **28**, 2185 (1992).
[12] K. Tamura, H. A. Haus, and E. P. Ippen, Electron. Lett. **28**, 2226 (1992).
[13] K. Tamura, E. P. Ippen, H. A. Haus, and L. E. Nelson, Opt. Lett. **18**, 1080 (1993).
[14] K. Tamura, C. R. Doerr, L. E. Nelson, H. A. Haus, and E. P. Ippen, Opt. Lett. **19**, 46 (1994).
[15] K. S. Abedin, J. T. Gopinath, L. A. Jiang, M. E. Grein, H. A. Haus, and E. P. Ippen, Opt. Lett. **27**, 1758 (2002).
[16] D. Y. Tang, W. S. Man, and H. Y. Tam, Opt. Commun. **165**, 189 (1999).
[17] C. Y. Wang, W. Zhang, K. F. Lee, and K. M. Yoo, Opt. Commun. **137**, 89 (1997).
[18] M. Lai, J. Nicholson, and W. Rudolph, Opt. Commun. **142**, 45 (1997).
[19] A. K. Komarov and K. P. Komarov, Opt. Commun. **183**, 265 (2000).
[20] A. K. Komarov and K. P. Komarov, Phys. Rev. E **62**, R7607 (2000).
[21] A. K. Komarov, K. P. Komarov, and A. S. Kuch'yanov, JETP Lett. **67**, 280 (1998); Pis'ma Zh. Eksp. Teor. Fiz. **67**, 261 (1998);
[22] D. Y. Tang, W. S. Man, H. Y. Tam, and P. D. Drummond, Phys. Rev. A **64**, 033814 (2001).
[23] Y. Gong, P. Shum, T. Hiang, Cheng, Q. Wen, and D. Tang, Opt. Commun. **200**, 389 (2001).
[24] D. Y. Tang, B. Zhao, D. Y. Shen, C. Lu, W. S. Man, and H. Y. Tam, Phys. Rev. A **66**, 033806 (2002).
[25] P. Grelu, F. Belhache, F. Gutty, and J.-M. Soto Crespo, Opt. Lett. **27**, 966 (2002).
[26] A. Hideur, B. Ortaç, T. Chartier, M. Brunel, H. Leblond, and F. Sanchez, Opt. Commun. **225**, 71 (2003).
[27] P. Grelu and J.-M. Soto Crespo, J. Opt. B: Quantum Semiclassical Opt. **6**, 271 (2004).
[28] B. Ortaç, A. Hideur, T. Chartier, M. Brunel, P. Grelu, H. Leblond, and F. Sanchez, IEEE Photonics Technol. Lett. **16**, 1274 (2004).
[29] N. H. Seong and D. Y. Kim, Opt. Lett. **27**, 1321 (2002).
[30] Y. D. Gong, P. Shum, D. Y. Tang, C. Lu, Z. W. Qi, W. J. Lai, W. S. Man, and H. Y. Tam, Opt. Commun. **220**, 297 (2003).
[31] M. E. Fermann, Appl. Phys. B: Lasers Opt. **58**, 197 (1994).
[32] M. E. Fermann, A. Galvanauskas, G. Sucha, and D. Harter, Appl. Phys. B: Lasers Opt. **65**, 259 (1997).
[33] H. A. Haus, J. G. Fujimoto, and E. P. Ippen, J. Opt. Soc. Am. B **8**, 2068 (1991).
[34] H. A. Haus, J. G. Fujimoto, and E. P. Ippen, IEEE J. Quantum Electron. **28**, 2086 (1992).
[35] H. A. Haus, E. P. Ippen, and K. Tamura, IEEE J. Quantum Electron. **30**, 200 (1994).
[36] E. P. Ippen, Appl. Phys. B: Lasers Opt. **58**, 159 (1994).
[37] L. E. Nelson, D. J. Jones, K. Tamura, H. A. Haus, and E. P. Ippen, Appl. Phys. B: Lasers Opt. **65**, 277 (1997).
[38] A. D. Kim, J. N. Kutz, and D. J. Muraki, IEEE J. Quantum

Electron. **36**, 465 (2000).
[39] K. M. Spaulding, D. H. Yong, A. D. Kim, and J. N. Kutz, J. Opt. Soc. Am. B **19**, 1045 (2002).
[40] H. Leblond, M. Salhi, A. Hideur, T. Chartier, M. Brunel, and F. Sanchez, Phys. Rev. A **65**, 063811 (2002).
[41] M. Salhi, H. Leblond, and F. Sanchez, Phys. Rev. A **67**, 013802 (2003).
[42] M. Salhi, H. Leblond, and F. Sanchez, Phys. Rev. A **68**, 033815 (2003).
[43] N. N. Akhmediev, A. Ankiewicz, and J.-M. Soto-Crespo, Phys. Rev. Lett. **79**, 4047 (1997).
[44] N. N. Akhmediev, A. Ankiewicz, and J.-M. Soto-Crespo, J. Opt. Soc. Am. B **15**, 515 (1998).
[45] P. Grelu, F. Belhache, F. Gutty, and J.-M. Soto-Crespo, J. Opt. Soc. Am. B **20**, 863 (2003).
[46] A. Hideur, T. Chartier, M. Brunel, M. Salhi, C. Özkul, and F. Sanchez, Opt. Commun. **198**, 141 (2001).
[47] G. P. Agrawal, *Nonlinear Fiber Optics*, 2nd Ed. (Academic Press, New York, 1995).
[48] A. K. Komarov, K. P. Komarov, and F. M. Mitschke, Phys. Rev. A **65**, 053803 (2002).